IEEE Access
Multidisciplinary | Rapid Review | Open Access Journal

Received March 8, 2019, accepted March 31, 2019, date of publication April 9, 2019, date of current version April 18, 2019.

Digital Object Identifier 10.1109/ACCESS.2019.2909589

Short-Range Reentry Guidance With Impact Angle and Impact Velocity Constraints for Hypersonic Gliding Reentry Vehicle

RONGGANG WANG, SHUO TANG, AND DONG ZHANG
School of Astronautics, Northwestern Polytechnical University, Xi'an 710072, China
Shaanxi Key Laboratory of Aerospace Flight Vehicle Technology, Northwestern Polytechnical University, Xi'an 710072, China

Corresponding author: Ronggang Wang (nwpuwrg@mail.nwpu.edu.cn)

This work was supported in part by the National Natural Science Foundation of China under Grant 11672235, and in part by the Defense Basic Research Program of China under Grant A0420132102.

ABSTRACT In order to ensure the normal operation of the guidance system and achieve precise reentry strike, it is necessary to complete the reentry guidance in a very short range of several hundred kilometers. Furthermore, the process constraints, including the field of view and overload, and the terminal constraints, such as the impact velocity and impact angle, need to be met. To solve these problems, a guidance strategy for short-range gliding with maneuvering deceleration capability is proposed. First, the flight-path angle command is generated in real time using a reference trajectory in the longitudinal plane of the gliding flight phase to ensure the timely convergence of the trajectory and meet the handover conditions. Second, in the terminal attack phase, a weight coefficient of the angle control command is introduced and adjusted according to the vertical field-of-view deviation to force down the trajectory and maintain the field-of-view constraint. Finally, the deceleration angle of attack and the additional angle of attack are selected as the control variables, and the deceleration requirements of the gliding flight phase and the terminal attack phase are met using the predictor–corrector method. The numerical simulations verify that the proposed guidance strategy exhibit good guidance performance and robustness.

INDEX TERMS Hypersonic gliding reentry vehicle, short-range reentry guidance, impact angle constraint, impact velocity constraint.

I. INTRODUCTION

Hypersonic gliding reentry vehicle (HGRV) has a very high speed and adopts an irregular gliding trajectory. It has a strong maneuverability and its trajectory is difficult to predict. As a result, it has become the latest choice in the breakthrough of the air defense and antimissile system. For the reentry guidance system to work properly, the impact velocity of the vehicle should not be too high. Excessive velocity not only increases the overload of the vehicle that adversely affects the accurate impact on the target, but also causes the vehicle to be surrounded by a plasma that is generated by the severe aerodynamic heating. As a consequence, the signal cannot be transmitted and refractive distortion can occur in the infrared barrier and the radome. It may even lead to serious consequences such as the destruction of the seeker structure, making it unable to work properly. Therefore, the realization of velocity control of the vehicle during the reentry phase using an appropriate maneuvering method that ensures the normal operation of the vehicle detection system and reduces the required overload, is the core to achieve an accurate reentry strike.

At present, the main methods of reentry guidance include nominal trajectory guidance [1]–[3] and predictor corrector guidance [4]–[6]. Although the nominal trajectory guidance has been applied in engineering practice, the accuracy of this method is greatly affected by the initial reentry error and environment disturbances, which makes it difficult to meet the requirements of a precision strike. Predictor corrector is further divided into analytical method [7], [8] and numerical method [9]–[13]. Analytical method is small in computational complexity and thus is convenient for engineering application. However, this method has large prediction model error, low guidance precision, weak constraint processing

The associate editor coordinating the review of this manuscript and approving it for publication was Ailong Wu.

ability and poor robustness. On the contrary, the numerical method does not have these problems, and is also insensitive to the initial values. But it also faces following challenges: (1) Converting the terminal altitude and velocity constraints into the terminal energy constraint can only accurately constrain the terminal energy, but is unable to strictly constrain the terminal altitude and velocity; (2) The pre-given angle of attack scheme based on velocity function is used to control the flight path only by the bank angle, which often leads to low control efficiency;(3) The trajectory prediction is greatly affected by the model error. Especially when the vehicle is close to the target and the dynamic pressure of the vehicle is very large, there is a possibility of the vehicle to lose the ability to correct the error and various random disturbances. In addition, the above reentry guidance schemes are mainly applied to the medium-long range reentry guidance of thousands of kilometers or more, and the feasibility of short-range reentry guidance problem within 500 km needs a further study.

In the terminal attack phase, the flight time is very short and the guidance pressure is very high, which is directly related to the success or failure of the mission. Meanwhile, the terminal guidance law need to consider the constraints of impact angle and impact velocity [14], [15]. At present, the deceleration guidance scheme in the terminal attack phase mainly includes the ideal velocity curve method [16] and the numerical predictor corrector method [17]–[20]. Their core ideas are to increase the induced drag to achieve energy consumption of the vehicle. The ideal velocity curve deceleration algorithm belongs to an analytical form of the predictor corrector algorithm, which is simple and has been tested in the engineering practice. The numerical predictor corrector method has a high control precision for the impact velocity and the impact angle, as well as exhibits a good robustness. However, there are also many problems with the above schemes, such as: (1) The prediction model of the ideal velocity curve deceleration guidance scheme has a large error, resulting in the low accuracy of controlling the impact velocity, and poor robustness; (2) The above deceleration guidance schemes do not consider the transition between the gliding flight phase and the terminal attack phase. Furthermore, they do not consider the guidance under the process constraint conditions such as the overload, field of view, as well as the coordination between the angle control command and the deceleration control command. For the impact angle constrained problem, there are two main ways to solve it: (1) The impact angle control can be achieve by adjusting the navigation coefficient [21], [22]; (2) On the basis of PN guidance law, the impact angle control can be achieved by designing an additional term [23], [24]. However, under the conditions of hypersonic flight and complex process constraints, and considering the effect of maneuvering deceleration, these methods are difficult to coordinate different guidance commands and achieve impact angle control in a limited time.

To solve the above problems, a hypersonic short-range reentry guidance strategy with a maneuvering deceleration capability is proposed. In the reentry gliding phase, a reference trajectory in the velocity-altitude space is designed, and the flight-path angle command is generated in real time according to it to complete the longitudinal guidance. In the lateral plane, the predictor corrector guidance is achieved with the deceleration angle of attack as the correction control variable, to obtain the lateral guidance command. The magnitude of the deceleration angle of attack is estimated based on the range and the velocity variation, in order to limit the search interval and speed up the search. In the terminal attack phase, a generalized biased PN algorithm is formulated and combined with the predictor corrector method to complete the entire terminal guidance by following means: (1) The guidance algorithm is improved to increase the guidance performance against the moving target by compensating the target motion information; (2) The weight coefficient is adjusted by the vertical field of view deviation to force down the trajectory and give a stable field of view tracking; (3) Predictor corrector guidance is performed with the designed additional angle of attack profile as the corrected control variable, and the precise control of the impact velocity is completed while ensuring the convergence of the trajectory; (4) The reference trajectory planned in the velocity-altitude space is used to estimate the initial value of the additional angle of attack in order to limit the search interval and speed up the search.

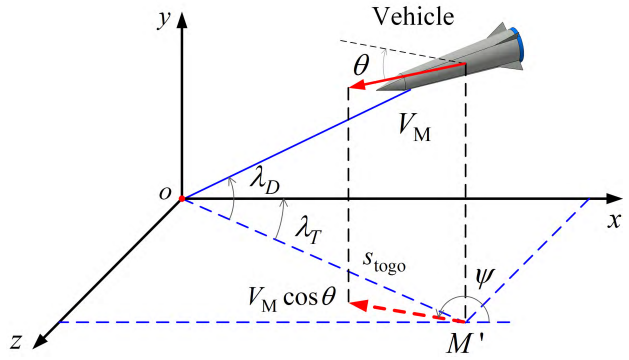

FIGURE 1. Engagement geometry and parameter definitions.

The rest paper is organized as follows. In Section II, the problem statement is described. In Section III, the short-range reentry gliding guidance algorithm is formulated. In Section IV, the terminal guidance scheme is presented. In Section V, the simulation results are given to illustrate the characteristics of the proposed guidance schemes. Finally, Section VI concludes the paper with a discussion on possible generalizations of this approach.

II. PROBLEM STATEMENT

In this paper, the Pershing II HGRV [16] is used as the research object. It can be assumed that the earth is a non-rotating homogeneous sphere. As shown in Fig.1, consider a 3-D engagement geometry. The target is at the origin of the coordinate system. The line of sight (LOS) is described by the azimuth angle λ_T and the elevation angle λ_D.

The angels θ and ψ represent the flight-path angle and the heading angle, respectively. For a detailed description of engagement geometry, the reader is referred to [25]. According to the engagement geometry, the 3-D equations of motion of HGRV are given by

$$\dot{x}_{\mathrm{M}} = V_{\mathrm{M}} \cos\theta \sin\psi \tag{1}$$

$$\dot{h} = V_{\mathrm{M}} \sin\theta \tag{2}$$

$$\dot{z}_{\mathrm{M}} = -V_{\mathrm{M}} \cos\theta \sin\psi \tag{3}$$

$$\dot{V}_{\mathrm{M}} = -\frac{D}{m} - g\sin\theta \tag{4}$$

$$\dot{\theta} = \frac{L}{mV_{\mathrm{M}}}\cos\sigma - \frac{Z}{mV_{\mathrm{M}}}\sin\sigma + \frac{1}{V_{\mathrm{M}}}\left(\frac{V_{\mathrm{M}}^2}{R} - g\right)\cos\theta \tag{5}$$

$$\dot{\psi} = -\frac{L}{mV_{\mathrm{M}}\cos\theta}\sin\sigma - \frac{Z}{mV_{\mathrm{M}}\cos\theta}\cos\sigma \tag{6}$$

$$R = h + R_0 \tag{7}$$

where R is the radial distance from the Earth center to the vehicle, R_0 is the equatorial radius of the Earth, and L, D and Z are the aerodynamic lift, drag and slide forces, respectively.

In addition, $\dot{\gamma}_{\mathrm{T}}$ and $\dot{\gamma}_{\mathrm{D}}$ are projections of the angular velocity of the velocity vector of HGRV on the longitudinal and lateral planes in LOS coordinate system. If $\dot{\gamma}_{\mathrm{T}}$ and $\dot{\gamma}_{\mathrm{D}}$ are known, $\dot{\theta}$ and $\dot{\psi}$ can be derived with the help of the knowledge in [25] as

$$\dot{\theta} = -\frac{\dot{\gamma}_{\mathrm{D}}}{\cos\left(\lambda_{\mathrm{T}} - \psi\right)} \tag{8}$$

$$\dot{\psi} = \frac{1}{\cos\lambda_{\mathrm{D}}}\left[\dot{\gamma}_{\mathrm{T}} - \dot{\gamma}_{\mathrm{D}}\tan\left(\lambda_{\mathrm{T}} - \psi\right)\sin\lambda_{\mathrm{D}}\right] \tag{9}$$

When the vehicle hits the target, the terminal constraints should be respectively expressed as

$$-90^\circ \le \theta\left(t_{\mathrm{f}}\right) \le -70^\circ \tag{10}$$

$$550\mathrm{m/s} \le V_{\mathrm{M}}\left(t_{\mathrm{f}}\right) \le 650\mathrm{m/s} \tag{11}$$

$$r\left(t_{\mathrm{f}}\right) \le 6\mathrm{m} \tag{12}$$

where r is the relative distance between the vehicle and the target.

Similar to the long-range gliding flight, the trajectory of the short-range can be divided into three phases: initial descent phase, gliding flight phase and terminal attack phase. The initial descent phase is to pull the vehicle up in time to prevent the vehicle from flying too low or hitting the ground. The gliding flight phase mainly reduces the velocity of the vehicle by a large margin under process constraints such as overload and heading field of view, and satisfies the handover point constraints such as the range-to-go, altitude and velocity. In this paper, the initial descent phase and the gliding flight phase are classified as the reentry gliding phase. The terminal attack phase is mainly to make the vehicle complete forcing down the trajectory under the process constraints, and satisfies the constraints of miss distance, impact angle and impact velocity. In Fig. 2, the flow chart of the guidance strategy proposed in this paper is given, and the detailed scheme is given later. The handover point used in this paper indicates the point at the interface of the terminal attack phase.

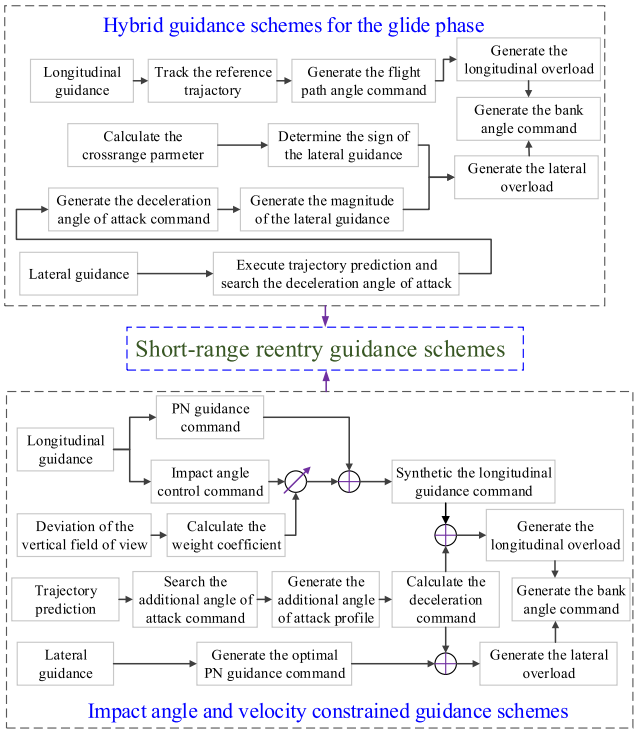

FIGURE 2. Block diagram of the short-range reentry guidance algorithm.

In the reentry gliding phase, the nominal trajectory guidance method and the predictor corrector guidance method are combined to solve the short-range reentry gliding guidance problem. In the longitudinal plane, a reference trajectory is planned in the velocity-altitude space to generate the flight-path angle command and achieve the constraints of altitude and range-to-go at the handover point. In the lateral plane, a deceleration angle of attack is introduced and used as the control variable to complete the predictor corrector guidance, which can achieve the velocity constraint at the handover point. In the terminal attack phase, a biased PN guidance law is formulated to satisfy the miss distance and impact angle constraints. The weight coefficient of the bias term can be adjusted adaptively to coordinate the PN command and the impact angle control command, in order to complete forcing down the trajectory and satisfy the field-of-view constraint. Meanwhile, the additional angle of attack is used as the control variable to complete the predictor corrector guidance and achieve the impact velocity constraint. To ensure the timely convergence of terminal guidance commands, the deceleration angle of attack profile is also designed.

III. DESIGN OF THE SHORT-RANGE REENTRY GLIDING GUIDANCE SCHEME

The traditional nominal trajectory guidance method and the predictor corrector guidance method have their own individual advantages and disadvantages. Due to the diversity of the requirements of the new reentry mission, a single method is

difficult to meet the design requirements. Thus, it is necessary to combine the two methods to give full play of their respective advantages. For the short-range reentry gliding phase, a hybrid guidance scheme is proposed. Firstly, the reference trajectory is planned in the velocity-altitude space, and the flight-path angle command is generated in real time to ensure the timely convergence of the trajectory and meet the altitude and the range-to-go requirements at the handover point. Subsequently, the predictor corrector method is performed with the deceleration angle of attack as the control variable in the lateral plane, and the search interval of the control variable is limited to improve the search speed while ensuring the deceleration accuracy. Finally, the crossrange boundary is restricted by the heading field of the view constraint, which provides the judgment condition for the bank reversal.

A. DERIVATION OF THE LONGITUDIAL GUIDANCE ALGORITHM

In the terminal attack phase, the flight time is very short. Precise velocity control should be achieved on the premise of satisfying miss distance and impact angle constraints. The deceleration capacity is very limited. Therefore, it is necessary to make the vehicle decelerate substantially in the gliding flight phase, so that the deceleration pressure can be greatly reduced in the terminal attack phase. At the handover point, the trajectory must have the correct conditions to ensure that successful approach flight is possible. The typical terminal conditions for reentry gliding phase are on altitude, velocity, and range-to-go, which are denoted as V_{MF}, h_{MF} and s_{MF}, respectively.

In dimensionless form, length is normalized by the equatorial radius of the Earth $R_0 = 6,378,135$ m, and time is normalized by $\sqrt{R_0/g_0}$ (where $g_0 = 9.81$ m/s^2); thus, velocity is normalized by $\sqrt{R_0/g_0}$. The terms L and D are the aerodynamic lift and drag acceleration in the unit of g_0, respectively. Then Eqs. (2) and (4) can be rewritten as

$$\bar{h}' = \bar{V}_{\mathrm{M}} \sin\theta \tag{13}$$

$$\bar{V}_{\mathrm{M}}' = -\bar{D} - \frac{\sin\theta}{\left(1+\bar{h}\right)^2} \tag{14}$$

As shown in Fig. 3, in the velocity-altitude space, a reference trajectory is designed by connecting the current point with the handover point. According to the scheme, in the entry phase, the vehicle is expected to be able to align from the current position to the end position of the glide phase. Then the flight-path angle command can be expressed as

$$\theta_c = -\arctan\left(\frac{h - h_{\mathrm{MF}}}{s_{\mathrm{togo}} - s_{\mathrm{MF}}}\right) \tag{15}$$

where s_{togo} represent the range-to-go, defined to be the range from the vehicle position to the target point. When $h \le h_{\mathrm{MF}}$ or $s_{\mathrm{togo}} < s_{\mathrm{MF}}$, the reentry gliding guidance is completed.

With the help of Eq. (15), the change rate of vertical projection of the velocity vector in the longitudinal plane can be designed using the tracking method as

$$\dot{\gamma}_{\mathrm{BD}} = -N\left(\theta - \theta_c\right) \tag{16}$$

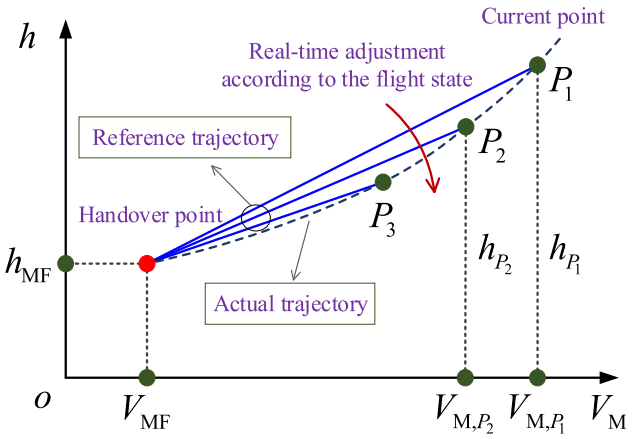

FIGURE 3. Design scheme of the reference trajectory.

During the reentry gliding phase, the altitude and velocity can be observed and controlled accurately. Therefore, the significance of trajectory planning in the velocity-altitude space is very intuitive. According to Fig. 3, the slope of the reference trajectory in the velocity-altitude space is given by

$$\left(\frac{\mathrm{d}\bar{h}}{\mathrm{d}\bar{V}_{\mathrm{M}}}\right)_{\mathrm{HG}} = \frac{\bar{h} - \bar{h}_{\mathrm{MF}}}{\bar{V}_{\mathrm{M}} - \bar{V}_{\mathrm{MF}}} \tag{17}$$

In the initial descent phase, it hopes that the trajectory of the vehicle can be pulled up as soon as possible, so that the reference trajectory can be tracked. Therefore, the stopping condition of the initial descent phase selected is

$$\delta = \left|\left(\frac{\mathrm{d}\bar{h}}{\mathrm{d}\bar{V}_{\mathrm{M}}}\right)_{\mathrm{3DOF}} - \left(\frac{\mathrm{d}\bar{h}}{\mathrm{d}\bar{V}_{\mathrm{M}}}\right)_{\mathrm{HG}}\right| \le \delta_{\mathrm{HG}} \tag{18}$$

where δ_{HG} is a small preselected positive number, and

$$\left(\frac{\mathrm{d}\bar{h}}{\mathrm{d}\bar{V}_{\mathrm{M}}}\right)_{\mathrm{3DOF}} = \frac{\bar{V}_{\mathrm{M}} \sin\theta}{-\bar{D} - \sin\theta \Big/ \left(1+\bar{h}\right)^2} \tag{19}$$

which is obtained by dividing Eq. (13) for $\bar{h}'$ with Eq. (14) for $\bar{V}_{\mathrm{M}}'$. The term in Eq. (19) represents the slope of the descending trajectory in the velocity-altitude space at any given ($\bar{V}_{\mathrm{M}}$,$\bar{h}$). The condition in Eq. (18) indicates a point at which the actual trajectory has the same slope as that of the reference trajectory at that velocity. Such a point is chosen to be the end of the initial descent so as to set up a smooth transition by the reentry trajectory into the gliding flight phase.

B. FORMULATION OF THE LATERAL GUIDANCE ALGORITHM

In the initial descent phase, the lateral guidance law is mainly used to reduce the initial crossrange. Therefore, the lateral guidance law in the initial descent phase can be expressed as

$$\dot{\gamma}_{\mathrm{BT}} = -N\Delta\psi \tag{20}$$

where $\Delta\psi = \psi - \Psi$ and Ψ is the azimuth angle of the vehicle from the current point to the direction of the target point.

As the altitude of the vehicle decreases and the dynamic pressure increases, the vehicle has sufficient ability to change its flight state. At the end of the initial descent phase, besides pulling up the actual trajectory as soon as possible, it is hoped that the actual trajectory can gradually keep up with the reference trajectory in velocity-altitude space. That is to say, the slope of the actual trajectory is approximately equal to that of the reference trajectory:

$$\left(\frac{\mathrm{d}\bar{h}}{\mathrm{d}\bar{V}_{\mathrm{M}}}\right)_{\mathrm{3DOF}} = \frac{\bar{V}_{\mathrm{M}}\sin\theta_c}{-\bar{D} - \sin\theta_c \Big/ \left(1+\bar{h}\right)^2} = \left(\frac{\mathrm{d}\bar{h}}{\mathrm{d}\bar{V}_{\mathrm{M}}}\right)_{\mathrm{HG}} \tag{21}$$

The angle of attack α enters in L and D through the dependence on α by the lift and drag coefficients C_L and C_D. Through the previous equation, the magnitude of the angle of attack needed to track the reference trajectory can be obtained as

$$\alpha = \sqrt{\left(-\frac{2\mu_2 m}{\rho_0 e^{-\beta h}\bar{V}_{\mathrm{M}}^2 S_{\mathrm{ref}} R_0} - C_{\mathrm{D0}}\right) \Big/ C_{\mathrm{D}}^{\alpha}} \tag{22}$$

where

$$\mu_2 = \left(\bar{V}_{\mathrm{M}}\sin\theta_c + \frac{\sin\theta_c}{\left(1+\bar{h}\right)^2}\left(\frac{\mathrm{d}\bar{h}}{\mathrm{d}\bar{V}_{\mathrm{M}}}\right)_{\mathrm{HG}}\right) \Big/ \left(\frac{\mathrm{d}\bar{h}}{\mathrm{d}\bar{V}_{\mathrm{M}}}\right)_{\mathrm{HG}} \tag{23}$$

At the end of the initial descent phase, because of the large dynamic pressure and the small balance angle of attack, the angle α obtained by Eq. (22) is mainly used for velocity control. Therefore, it can be directly used as the deceleration angle of attack command $\tilde{\alpha}$ for lateral guidance.

In the reentry gliding phase, the magnitude of the lateral guidance command in this paper can be expressed as

$$\dot{\gamma}_{\mathrm{BT}} = \frac{\rho_0 e^{-\beta h} V_{\mathrm{M}} S_{\mathrm{ref}}}{2m} C_{\mathrm{L}}^{\alpha}\tilde{\alpha} \tag{24}$$

According to Eq. (24), to determine the magnitude of the lateral guidance command, the calculation of deceleration angle of attack is also the key. Equation(22) can be used directly as the deceleration angle of attack. Obviously, it is an analytical predictor corrector method and has the common problems of the analytical method. In addition, the variation of the deceleration angle of attack obtained by Eq. (22) is relatively large. It is not conducive to the stability of the guidance and control system. Thus the numerical predictor corrector method is used to calculate the deceleration angle of attack in the gliding flight phase.

The magnitude of a constant deceleration angle of attack is iteratively sought to meet the terminal velocity constraint at the interface of the terminal attack phase. For any such a deceleration angle of attack, the sign is determined by the lateral logic to be discussed later. With the magnitude and sign of the deceleration angle of attack specified, the dynamic Eqs. (1-6) are numerically integrated form the current condition to s_{MF}. The predicted $V_{\mathrm{M}}(s_{\mathrm{MF}})$ is then compared to V_{MF}, and the mismatch is used to adjust $\tilde{\alpha}$. A secant method below is found to be effective toward this purpose:

$$\tilde{\alpha}_{k+1} = \tilde{\alpha}_k - \frac{\tilde{\alpha}_k - \tilde{\alpha}_{k-1}}{\Delta V_{\mathrm{MF}}^k - \Delta V_{\mathrm{MF}}^{k-1}}\Delta V_{\mathrm{MF}}^k \tag{25}$$

where

$$\Delta V_{\mathrm{MF}} = V\left(\tilde{\alpha}_k, s_{\mathrm{MF}}\right) - V_{\mathrm{MF}} \tag{26}$$

Once the correct $\tilde{\alpha}$ is found, the magnitude of the lateral guidance command $|\dot{\gamma}_{\mathrm{BT}}|$ is specified.

When using secant method to search deceleration angle of attack $\tilde{\alpha}$, search interval has a great influence on search speed. If the search interval can be limited to a small range, it will greatly improve the search speed. It can be shown that the differential equation for s_{togo} is

$$\dot{s}_{\mathrm{togo}} = -V_{\mathrm{M}}\cos\theta\cos\Delta\psi \tag{27}$$

With the approximation $\Delta\psi \approx 0$, the expression of range-to-go s_{togo} can be approximately simplified to

$$\dot{s}_{\mathrm{togo}} = -V_{\mathrm{M}}\cos\theta \tag{28}$$

Dividing Eq. (4) by Eq. (28) results in

$$\frac{\mathrm{d}V_{\mathrm{M}}}{\mathrm{d}s_{\mathrm{togo}}} = \frac{0.5C_{\mathrm{D}}\rho_0 e^{-\beta h}V_{\mathrm{M}}S_{\mathrm{ref}}}{m\cos\theta} + \frac{g}{V_{\mathrm{M}}}\tan\theta \tag{29}$$

If the gravity term in Eq. (29) is ignored, it can be readily shown that

$$\frac{\mathrm{d}V_{\mathrm{M}}}{\mathrm{d}s_{\mathrm{togo}}} \approx \frac{0.5C_{\mathrm{D}}\rho_0 e^{-\beta h}V_{\mathrm{M}}S_{\mathrm{ref}}}{m\cos\theta} \tag{30}$$

In order to integrate Eq. (30) and obtain the direct relationship between the velocity and the range-to-go, it is necessary to establish the relationship between the altitude and the range-to-go. In this paper, we hope that the actual trajectory of the vehicle can keep up with the reference trajectory, that is, the expected flight altitude of the vehicle is approximately linear with the range-to-go, which can be described as

$$h = k_1 s_{\mathrm{togo}} + k_2 \tag{31}$$

where k_1 and k_2 are design parameters. If the data $(s_{\mathrm{MF}}, h_{\mathrm{MF}})$ and $\left(s_{\mathrm{togo}}^{t_i}, h^{t_i}\right)$ corresponding to the handover point and time t_i are known, substituting them into Eq. (31) can be obtained as

$$k_1 = \frac{h_{t_i} - h_{\mathrm{MF}}}{s_{\mathrm{togo},t_i} - s_{\mathrm{MF}}} \tag{32}$$

$$k_2 = h_{\mathrm{MF}} - \frac{h_{t_i} - h_{\mathrm{MF}}}{s_{\mathrm{togo},t_i} - s_{\mathrm{MF}}}s_{\mathrm{MF}} \tag{33}$$

Substituting Eq. (31) into Eq. (30) and integrating it can get

$$C_{\mathrm{D}} = \frac{\beta k_1 m\cos\theta_c}{\rho_0 S_{\mathrm{ref}} e^{-\beta k_2}\left(e^{-\beta k_1 s_{\mathrm{MF}}} - e^{-\beta k_1 s}\right)}\ln\left(\frac{V_{\mathrm{M}}}{V_{\mathrm{MF}}}\right)^2 \tag{34}$$

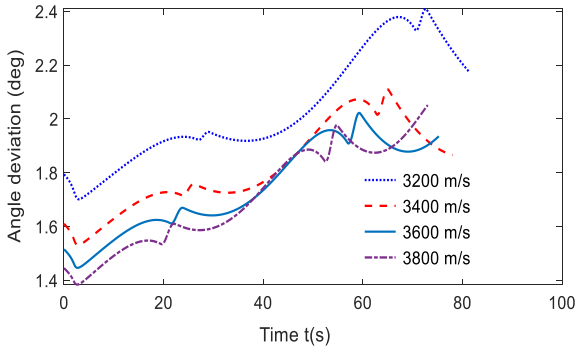

FIGURE 4. Deviations between the estimated value and the theoretical value of the deceleration angle of attack.

By solving the above equation, the approximate deceleration angle of attack can be obtained as follows:

$$\tilde{\alpha} = \sqrt{\frac{2}{\rho_0 S_{\text{ref}} e^{\beta k_2}} \frac{\beta k_1 m \cos\theta}{e^{-\beta k_1 s_{\text{MF}}} - e^{-\beta k_1 s}} \ln\left(\frac{V_{\text{M}}}{V_{\text{MF}}}\right) - C_{\text{D0}}}{C_{\text{D}}^{\alpha}}} \tag{35}$$

Figure 4 shows the time-varying curves of deceleration angle of attack deviation between the estimated value obtained by Eq. (35) and the theoretical value under different initial velocity conditions in the gliding flight phase. It can be seen that the error is less than 2.5 deg within 50 seconds. The results indicate that the proposed method gives accurate estimations of the initial deceleration angle of attack.

The next task is to determine the sign of the applied lateral command. According to the definition in [11], the crossrange parameter Z is given by

$$Z = \arcsin\left(\sin\left(\frac{s_{\text{togo}}}{R_0 + h}\right)\sin\Delta\psi\right) \tag{36}$$

The crossrange boundary can be expressed as follows:

$$Z_{\max} = \left|\arcsin\left(\sin\left(\frac{s_{\text{togo}}}{R_0 + h}\right)\sin\Delta\Psi_{\max}\right)\right| \tag{37}$$

Whenever the magnitude of the parameter $|Z|$ along the trajectory exceeds $Z_{\max}$, the sign of the lateral guidance command is reversed, and this sign is maintained until the condition $|Z| < Z_{\max}$ is again violated. The threshold value $\Delta\Psi_{\max}$, which is chosen to maintain the heading field of view.

For the reentry trajectory, the trajectory shape is determined by the flight range and the number of bank reversals. For the traditional long-range HGRV (such as the space shuttle), the number of bank reversals is mainly determined by the energy level, range and crossrange boundary of the vehicle, and its lateral trajectory shape is similar to S-shaped curve (as shown by the trajectory ② in Fig. 5). For the short-range HGRV studied in this paper, the corresponding number of bank reversals is related not only to the energy level and range, but also to the lateral field of view of the vehicle.

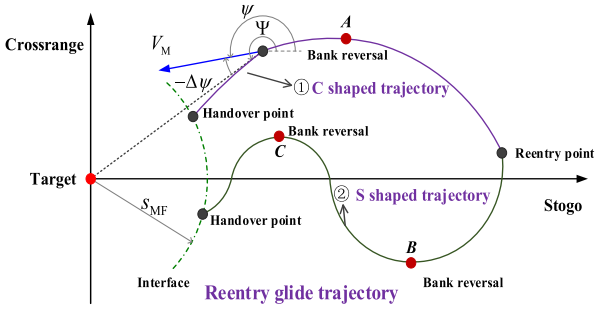

FIGURE 5. Characteristic analysis of the lateral reentry trajectory.

Because of its short reentry flight range and large seeker field of view, its reentry trajectory is similar to C-shaped curve (as shown by the trajectory ① in Fig. 5).

The acceleration model is mainly determined by the gravitational acceleration model and the aerodynamic acceleration model. The gravitational acceleration model can be obtained from the standard earth model. However, the uncertainty errors of atmospheric density, wind field and other parameters during reentry have a great influence on the acceleration of reentry gas. In order to predict the trajectory accurately, the standard atmospheric density model needs to be revised according to the actual flight state.

C. ON-LINE COMPENSATION SCHEME FOR ENVIRONMENTAL PARAMETERS

When the atmospheric density and drag coefficient exist big errors, it is difficult to satisfy the required terminal constraints. In this case, it is necessary to compensate the environmental parameters online.

The flight environment factors affecting aerodynamic force mainly include aerodynamic parameters and atmospheric density. However, the effects of aerodynamic parameters and atmospheric density cannot be determined separately without the aid of atmospheric data sensors. Therefore, the aerodynamic parameters and atmospheric density cannot be identified separately, only the combined effects can be determined. Based on the aerodynamic coefficient model, two comprehensive aerodynamic coefficients K_{L} and K_{D} are introduced, which can be defined respectively as

$$K_{\text{L}} = \rho C_{\text{D}} \tag{38}$$

$$K_{\text{D}} = \rho C_{\text{D}} \tag{39}$$

According to the inertial measurement devices of the vehicle, the combined acceleration of the vehicle a can be measured. Furthermore, the aerodynamic accelerations $\hat{a}_{\text{L}}$ and $\hat{a}_{\text{D}}$ in the direction of lift and drag can be obtained respectively as

$$\hat{a}_{\text{D}} = -\boldsymbol{a} \cdot i_{\text{V}} \tag{40}$$

$$\hat{a}_{\text{L}} = \sqrt{\boldsymbol{a} \cdot \boldsymbol{a} - \hat{a}_{\text{D}}^2} \tag{41}$$

where i_{V} is the unit vector of the velocity vector of the vehicle.

From Eqs. (38) and (41), we also have

$$K_{\mathrm{L}} = \frac{2\hat{a}_{\mathrm{L}}}{V_{\mathrm{M}}^2}\frac{m}{S_{\mathrm{ref}}} \tag{42}$$

Similarly,

$$K_{\mathrm{D}} = \frac{2\hat{a}_{\mathrm{D}}}{V_{\mathrm{M}}^2}\frac{m}{S_{\mathrm{ref}}} \tag{43}$$

The variables K_{L} and K_{D} can be used to compensate for the uncertainty errors of aerodynamic parameters and atmospheric density.

If we want to consider more complex conditions, or make the identification more accurate, the equations of motion can be used as the state equations for identification problem. According to the missile motion information obtained by inertial devices on the vehicle, the observation equations can be established. Then the EKF (Extended Kalman Filter) method or the RLS (Recursive Least-square) method can be used to identify the aerodynamic coefficients. For a detailed description of the specific method, the reader is referred to [26].

IV. DERIVATION OF THE TERMINAL GUIDANCE SCHEME

The terminal guidance scheme with impact angle and impact velocity constraints is proposed, as shown in Fig. 2. Firstly, a relative biased PN guidance algorithm with the target maneuver information compensation is derived to improve the guidance performance. Subsequently, a weight coefficient is introduced in the front of the angle control term, which is adjusted to force down the trajectory in time and maintain the vertical field of view constraint. Finally, by designing the additional angle of attack profile and using the numerical predictor corrector method, the trajectory can be converged in time and the velocity control accuracy can be ensured. The search speed in trajectory prediction is accelerated by restricting the additional angle of attack search interval.

A. FORMULATION OF THE IMPACT ANGLE CONSTRAINED GUIDANCE ALGORITHM

Although a number of guidance methods [27]–[31] can guide the vehicle to the target from a specific direction. However, these guidance schemes seldom consider hypersonic attack on ground targets, especially for moving targets. In addition, how to coordinate the angle control command and the PN guidance command under process constraints such as field of view to force down the trajectory smoothly is rarely considered. Figure 6 shows the relative motion between the vehicle and the target in the longitudinal plane of the terminal attack phase, where V_{R} and γ_{R} denote the relative velocity and the relative flight-path angle, respectively. It should be noted that the research object in this paper is to hit the ship at sea, which can be approximately regarded as a horizontal moving target.

In the longitudinal plane, the engagement kinematics can be approximately represented by the following

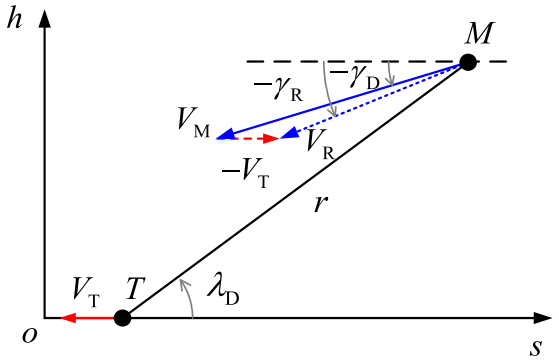

FIGURE 6. Engagement geometry in the longitudinal plane.

differential equations:

$$\dot{r} = V_{\mathrm{Ta}}\cos\lambda_{\mathrm{D}} - V_{\mathrm{M}}\cos\left(\gamma_{\mathrm{D}} + \lambda_{\mathrm{D}}\right) \tag{44}$$

$$r\dot{\lambda}_{\mathrm{D}} = V_{\mathrm{M}}\sin\left(\gamma_{\mathrm{D}} + \lambda_{\mathrm{D}}\right) - V_{\mathrm{T}}\sin\lambda_{\mathrm{D}} \tag{45}$$

The relative leading angle is defined as $\eta_{\mathrm{R}} = \gamma_{\mathrm{R}} + \lambda_{\mathrm{D}}$ for convenience. Then Eqs.(44) and (45) can be reduced to

$$\dot{r} = -V_{\mathrm{R}}\cos\eta_{\mathrm{R}} \tag{46}$$

$$r\dot{\lambda}_{\mathrm{D}} = V_{\mathrm{R}}\sin\eta_{\mathrm{R}} \tag{47}$$

Using Eqs.(44)-(47), the relative flight-path angle γ_{R} can be readily found to be

$$\gamma_{\mathrm{R}} = \tan^{-1}\left(\frac{\sin\gamma_{\mathrm{D}}}{\cos\gamma_{\mathrm{D}} - \beta}\right) \tag{48}$$

where $\beta = V_{\mathrm{T}}/V_{\mathrm{M}}$ is the target to missile ratio.

Although the velocity ratio is used, it is only used as a compensation coefficient because of its small influence. In addition, because the terminal velocity is specified, the actual velocity ratio is the projection of the velocity vector of HGRV to that of the target in the longitudinal plane, which is given by

$$\beta = \frac{V_T\cos\left(\psi_T - \Psi\right)}{\left|V_{MF}\cos\left(\psi - \Psi\right)\right|} \tag{49}$$

where ψ_{T} is the heading angle of the target.

The derivative of Eq. (48) is easily obtained as

$$\dot{\gamma}_{\mathrm{D}} = \kappa\cdot\dot{\gamma}_{\mathrm{R}} \tag{50}$$

where

$$\kappa = \frac{1 - 2\beta\cos\gamma_{\mathrm{D}} + \beta^2}{1 - \beta\cos\gamma_{\mathrm{D}}} \tag{51}$$

Due to $\beta \ll 1$, $1 - \beta\cos\gamma_{\mathrm{D}} > 0$ is always satisfied in the guidance process. In addition, we also have

$$1 - 2\beta\cos\gamma_{\mathrm{D}} + \beta^2 \geq (1 - \beta)^2 \tag{52}$$

Obviously, the numerator of Eq. (52) is a positive quantity for $\beta > 1$. Therefore, based on the preceding analysis, we know that κ will not occur singularity and satisfy the condition $\kappa > 0$ during the whole terminal attack phase.

The impact angle constrained guidance law mainly consists of two items: PN command, which is mainly used to reduce miss distance, and bias term, which is mainly used to control the impact angle. Considering the possibility of striking a moving target, the idea of the relative PN in [32] is introduced, which is described as

$$\dot{\gamma}_{\mathrm{R}} = -N\dot{\lambda}_{\mathrm{D}} + b \tag{53}$$

where N is the navigation constant and b is the bias term.

After integrating Eq. (53) from t to t_{f}, we

$$\gamma_{\mathrm{RF}} - \gamma_{\mathrm{R}} = -N\left(\lambda_{DF} - \lambda_{\mathrm{D}}\right) + \int_{t}^{t_{\mathrm{f}}} b d\tau \tag{54}$$

Assuming that b is constant throughout the guidance process, the approximate expression of b is obtained as

$$b = \frac{(1-N)\,\gamma_{\mathrm{RF}} - \gamma_{\mathrm{R}} - N\lambda_{\mathrm{D}}}{t_{\mathrm{go}}} \tag{55}$$

With Eqs.(50), (53) and (55), the specific form of the relative biased PN guidance can be obtained as

$$\dot{\gamma}_{\mathrm{D}} = \dot{\gamma}_{\mathrm{D,PN}} + \dot{\gamma}_{\mathrm{D,B}} \tag{56}$$

where

$$\dot{\gamma}_{\mathrm{D,PN}} = -\kappa N\dot{\lambda}_{\mathrm{D}} \tag{57}$$

$$\dot{\gamma}_{\mathrm{D,B}} = \kappa\frac{(1-N)\,\gamma_{\mathrm{RF}} - \gamma_{\mathrm{R}} - N\lambda_{\mathrm{D}}}{t_{\mathrm{go}}} \tag{58}$$

From gliding flight to terminal attack, $\dot{\lambda}_{\mathrm{D}} > 0$ is always satisfied in the middle and early stages of the terminal attack phase. Through the analysis of Eq. (57), it can be seen that $N > 1$ and $\kappa > 0$ is always satisfied during the terminal attack phase. From Eq. (58), it can be seen that $\dot{\gamma}_{\mathrm{D,PN}} < 0$ is always satisfied, that is, the PN command always forces down the trajectory of the vehicle. In addition, because of the need to strike the target vertically, we know $\gamma_{\mathrm{R}}\mathrm{F} \approx -\pi/2$. In the early stage of the terminal attack phase, because the flight-path angle is relatively small, we know $\dot{\gamma}_{\mathrm{D,B}} > 0$. That is to say, the trajectory may be pulled up after the impact angle control command is added. If the relationship between the PN term and the biased term is not well coordinated, the following four results may occur:

1) If the impact angle control command is too large, which will make it difficult for the vehicle to force down the trajectory under various constraints, and then lead to the failure of the guidance mission.

2) If the pull-up amplitude of the trajectory is too large, the target will be out of the field of view for a long time, as shown by the solid line in Fig. 7.

3) If the angle control command is too small in the early stage, the vehicle will not have enough magnitude of the impact angle in the middle and early stage, which will affect the accuracy of impact angle control, as shown by the broken line in Fig. 7.

Based on the preceding analysis, the PN guidance command and the impact angle control command should be coordinated reasonably in the whole terminal attack phase,

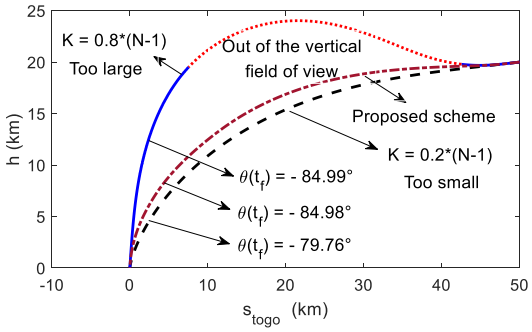

FIGURE 7. Effect of the angle control command on the trajectory.

so that the desired terminal velocity, impact angle and miss distance of the vehicle can be achieved under the required process constraints. In this paper, a variable angle deviation feedback coefficient scheme is adopted, in which a weight coefficient K is set in the front of the bias term, so that the relationship between the PN command and the angle control command can be coordinated well.

According to the above design idea,(53) can be changed into the following form:

$$\dot{\gamma}_{\mathrm{R}} = -N\dot{\lambda}_{\mathrm{D}} + K\frac{\varepsilon_{\mathrm{R}}}{t_{\mathrm{go}}} \tag{59}$$

where

$$\varepsilon_{\mathrm{R}} = (N-1)\,\lambda_{\mathrm{DF}} - \gamma_{\mathrm{R}} - N\lambda_{\mathrm{D}} \tag{60}$$

The derivative of Eq. (60) is obtained as

$$\dot{\varepsilon}_{\mathrm{R}} = -K\frac{\varepsilon_{\mathrm{R}}}{t_{\mathrm{go}}} \tag{61}$$

Let η_{R} be the derivative of time and divide it by Eq. (61). Then you can get

$$\frac{\mathrm{d}\eta_{\mathrm{R}}}{\mathrm{d}\varepsilon_{\mathrm{R}}} = \frac{(N-1)}{K}\frac{\sin\eta_{\mathrm{R}}}{\varepsilon_{\mathrm{R}}} - 1 \approx \frac{(N-1)}{K}\frac{\eta_{\mathrm{R}}}{\varepsilon_{\mathrm{R}}} - 1 \tag{62}$$

After the integral of Eq. (62), we can get

$$\eta_{\mathrm{R}} = c_0\varepsilon_{\mathrm{R}}^{\frac{N-1}{K}} + \frac{K}{N-K-1}\varepsilon_{\mathrm{R}} \tag{63}$$

where

$$c_0 = \left(\eta_{\mathrm{D0}} - \frac{K}{N-K-1}\varepsilon_{\mathrm{R0}}\right)\varepsilon_{\mathrm{R0}}^{-\frac{N-1}{K}} \tag{64}$$

The condition $0 \le \varepsilon_{\mathrm{R}} < 1$ will be always met during the whole terminal attack phase. From the analysis of Eq. (63), when $K < N-1$, the angle η_{R} will speed up convergence to zero as $\varepsilon_{\mathrm{R}} \to 0$. That is to say, in the middle and early stage, the impact angle control should be accelerated to converge, so as to reduce the later guidance pressure to ensure the guidance accuracy.

In this paper, K can be regarded as a penalty function. In the first half of the trajectory, K can be taken as a small value to force down the trajectory rapidly and stable the field of

view tracking. In the second half of the trajectory, the value of K can be gradually increased to complete the angle control as soon as possible. The variation of the trajectory can be measured by the vertical field of view deviation which is denoted as $q_\alpha = \theta + \lambda_D$. If the value of q_α is large, the trajectory fluctuates significantly, whereas the trajectory has small fluctuation. Therefore, according to the above analysis, K can be taken as the following form:

$$K = \begin{cases} 0, & if\ |q_\alpha| \geq q_{\alpha,\max}; \\ \left(\delta_{\max} - \delta_{\max}\dfrac{|q_\alpha|}{q_{\alpha,\max}}\right)(N-1), & if\ |q_\alpha| < q_{\alpha,\max}; \end{cases} \tag{65}$$

where $q_{\alpha,\max}$ is the boundary of the vertical field of view constraint, and $\delta_{\max}$ is the maximum design coefficient which satisfies $0 < \delta_{\max} < 1$.

B. DECELERATION CONTROL ALGORITHM

The reentry process of HGRV has certain limitations on the magnitude and direction of the velocity. Although the guidance law given in the previous subsection can achieve the control of the velocity direction, the control of the velocity is difficult to be achieved. A large deceleration of HGRV can only be achieved by increasing the angle of attack. It is necessary to increase the angle of attack and try to avoid the interference of the deceleration control command on the guidance command. To meet these requirements, an additional angle of attack may be added in the vertical direction of the guide angle of attack. It should be noted that the additional angle of attack is different from the deceleration angle of attack. The additional angle of attack is introduced to reduce the influence of deceleration maneuver on the guidance command, whereas the additional angle of attack is a virtual command which is used to generate the lateral guidance command.

The rotation rate of the velocity of the vehicle caused by the guidance angle of attack α_g with no consideration of deceleration maneuver is denoted as $\dot\gamma_g$, which is given by

$$\dot\gamma_g = \sqrt{\dot\gamma_D^2 + \dot\gamma_T^2} \tag{66}$$

The rotation rate of the velocity of the vehicle caused by the additional angle of attack α_N is denoted as $\Delta\dot\gamma$. The mechanism of the additional angle of attack α_N is to decelerate the vehicle by conical motion on the basis of the guidance trajectory, as shown in Fig. 8. According to the direction of the additional angle of attack α_N defined, the total velocity direction rotation rate $\dot\gamma_B$ is calculated as

$$\dot\gamma_B = \sqrt{\dot\gamma_g^2 + \Delta\dot\gamma^2} \tag{67}$$

According to the geometric relationship, it can be seen that after adding the additional angle of attack, the components of the velocity turning rate $\dot\gamma_{BD}$ and $\dot\gamma_{BT}$ in the longitudinal plane

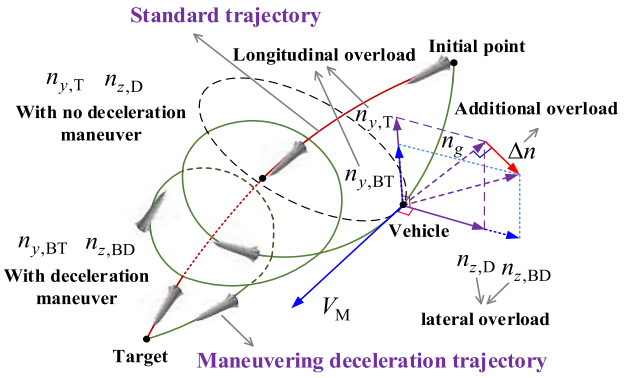

FIGURE 8. The sketch map of the deceleration trajectory.

and the lateral plane can be respectively expressed as

$$\dot\gamma_{BD} = \dot\gamma_D + \frac{\dot\gamma_T}{\dot\gamma_g}\Delta\dot\gamma, \quad \dot\gamma_{BT} = \dot\gamma_T - \frac{\dot\gamma_D}{\dot\gamma_g}\Delta\dot\gamma \tag{68}$$

In addition, $\Delta\dot\gamma$ can be calculated from the additional angle of attack α_N, which is described as

$$\Delta\dot\gamma = \frac{\rho V_M S_{ref}}{2m} C_L^\alpha \alpha_N \tag{69}$$

The additional angle of attack can be searched by numerical predictor-corrector method in the initial part of the terminal attack phase. The search algorithm can adopt secant method which can be expressed as

$$\tilde\alpha_{N,k+1} = \tilde\alpha_{N,k} - \frac{\tilde\alpha_{N,k} - \tilde\alpha_{N,k-1}}{\Delta V_F^k - \Delta V_F^{k-1}}\Delta V_F^k \tag{70}$$

$$\Delta V_F = V_M(h_F) - V_F \tag{71}$$

where V_F is the desired impact velocity and h_F is the expected impact height.

In the velocity-altitude space, the reference trajectory is based on the connection between the current point (V_M, h) and the desired terminal point (V_{MF}, h_{MF}). The slope of the desired trajectory in velocity-altitude space can be expressed as

$$\left(\frac{d\bar h}{d\bar V_M}\right)_{HT} = \frac{\bar h - \bar h_{MF}}{\bar V_M - \bar V_{MF}} \tag{72}$$

After trajectory stabilization, the slope in the velocity altitude space should be approximately equal to the slope of the reference trajectory:

$$\frac{\bar V_M \sin(-\lambda_D)}{-\bar D - \sin(-\lambda_D)/(1+\bar h)^2} = \left(\frac{d\bar h}{d\bar V_M}\right)_{HT} \tag{73}$$

Since α_g is not very large in the initial stage of the terminal attack phase, it can be approximately considered that the angle of attack obtained by Eq. (73) is the estimated value of the additional angle of attack. Its expression can be described as

$$\tilde\alpha_N = \sqrt{\left(\frac{2m\mu_1}{\rho_0 e^{-\beta h}\bar V_M S_{ref} R_0} - C_{D0}\right)\Big/ C_D^\alpha} \tag{74}$$

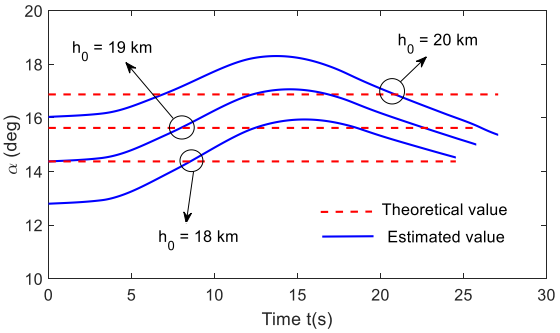

FIGURE 9. Comparison results between the estimated value and the theoretical value of the additional angle of attack.

where

$$\mu_1 = \left(\bar{V}_{\mathrm{M}} \sin\lambda_{\mathrm{D}} + \frac{\sin\lambda_{\mathrm{D}}}{(1+\bar{h})^2}\left(\frac{\mathrm{d}\bar{h}}{\mathrm{d}\bar{V}_{\mathrm{M}}}\right)_{\mathrm{HT}}\right) \Big/ \left(\frac{\mathrm{d}\bar{h}}{\mathrm{d}\bar{V}_{\mathrm{M}}}\right)_{\mathrm{HT}} \tag{75}$$

Figure 9 shows the comparison results between the additional angle of attack calculated by Eq. (74) and the theoretical value at different initial altitudes. It can be seen that the estimated deviation is less than 2 deg. The results indicate that the proposed method gives an accurate estimation of the initial additional angle of attack. Therefore, the angle $\tilde{\alpha}_{\mathrm{N}}$ obtained by Eq. (74) is used to reduce the search interval, in order to speed up the secant method given by Eq. (70).

In the terminal attack phase, the vehicle is very close to the target position, so its deceleration ability and maneuverability are very limited. As shown in Fig. 10, in order to ensure that the vehicle can accurately manage the surplus energy and minimize the interference to the terminal guidance system, the terminal attack phase can be divided into three compartments according to the altitude. In the first stage ($h_{\mathrm{T1}} \sim h_{\mathrm{MF}}$), the maximum deceleration is achieved by using the additional angle of attack obtained by the search algorithm (70), which only needs to be searched once. In the second stage ($h_{\mathrm{T2}} \sim h_{\mathrm{T1}}$), the main purpose is to gradually reduce the magnitude of the maneuvering deceleration, and prevent excessive maneuvering of the vehicle from making the guidance algorithm difficult to converge in time. In the non-deceleration stage, the main purpose is to ensure the precise execution of the impact angle control guidance without deceleration maneuver. Based on above discussion, the additional angle of attack profile in the terminal attack phase can be designed as the following form:

$$\alpha_N = \begin{cases} \alpha_{N,\max}, & h \geq h_{T_1}; \\ \dfrac{h_{T_1} - h}{h_{T_1} - h_{T_2}} \alpha_{N,\max}, & h_{T_2} \leq h < h_{T_1}; \\ 0, & h < h_{T_1}. \end{cases} \tag{76}$$

It should be noted that the velocity control algorithm proposed in this paper can only achieve deceleration, but not acceleration, which requires that in the reentry guidance process, the actual velocity of the missile is not less than the velocity command.

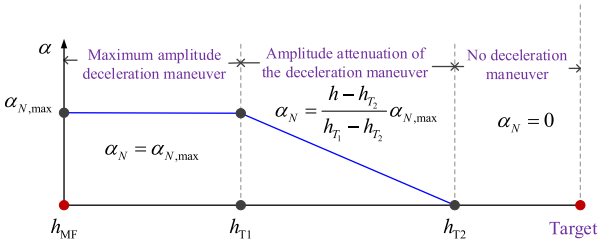

FIGURE 10. Additional angle of attack profile.

TABLE 1. Reentry constraint conditions.

Variable	Description	Value
$r(t_{\mathrm{f}})$	Miss distance (m)	<6
$V_{\mathrm{M}}(t_{\mathrm{f}})$	Impact velocity (m/s)	600
$\theta(t_{\mathrm{f}})$	Impact angle (deg)	-85
n_{yz}	Acceleration (g)	-25~25
q_α / q_β	Field of view (deg)	-30~30
α	Angle of attack (deg)	-25~25

V. SIMULATION RESULTS

In order to investigate the performance of the proposed guidance scheme, two sets of simulations are made. One set is only for the terminal attack phase without considering the reentry gliding phase. The other set for all the reentry trajectories, which include the initial descent, gliding flight and terminal attack. The reentry constraints are given in Table 1. To ensure the stability of the guidance and control system, and prevent the mutual interference of the guidance commands, the deceleration control is stopped to ensure the guidance accuracy of miss distance and impact angle constraint, when the altitude of the vehicle is less than 8 km.

A. GUIDANCE PERFORMANCE FOR THE TERMINAL ATTACK PHASE

In order to verify the performance of the proposed terminal attack guidance algorithm, the comparison results between the proposed guidance scheme (case 3), and the optimal guidance law (case 1) and the velocity control guidance algorithm (case 2) in [25] are given in Fig. 11. The initial conditions are given by Table 2. Compared with case 1 and case 2, it can be seen from Fig. 11a that the proposed guidance scheme decelerates mainly by coning motion, and the amplitude of the vehicle maneuver decreases gradually as the vehicle approaches the target, which corresponds to the additional angle of attack profile. It can be seen from Figs. 11b and 11c that the accuracy of the impact velocity and the impact angle of the proposed guidance scheme are 1.4 m/s and 0.03°, respectively. Since the relationship between the impact angle control command and the PN guidance command is not coordinated, both schemes 1 and 2 exceed the boundary of the vertical field of view, while the scheme 3 proposed in this paper satisfies the required field of view constraint (see Fig. 11d), and the acceleration also meets the requirement (see Fig. 11e).

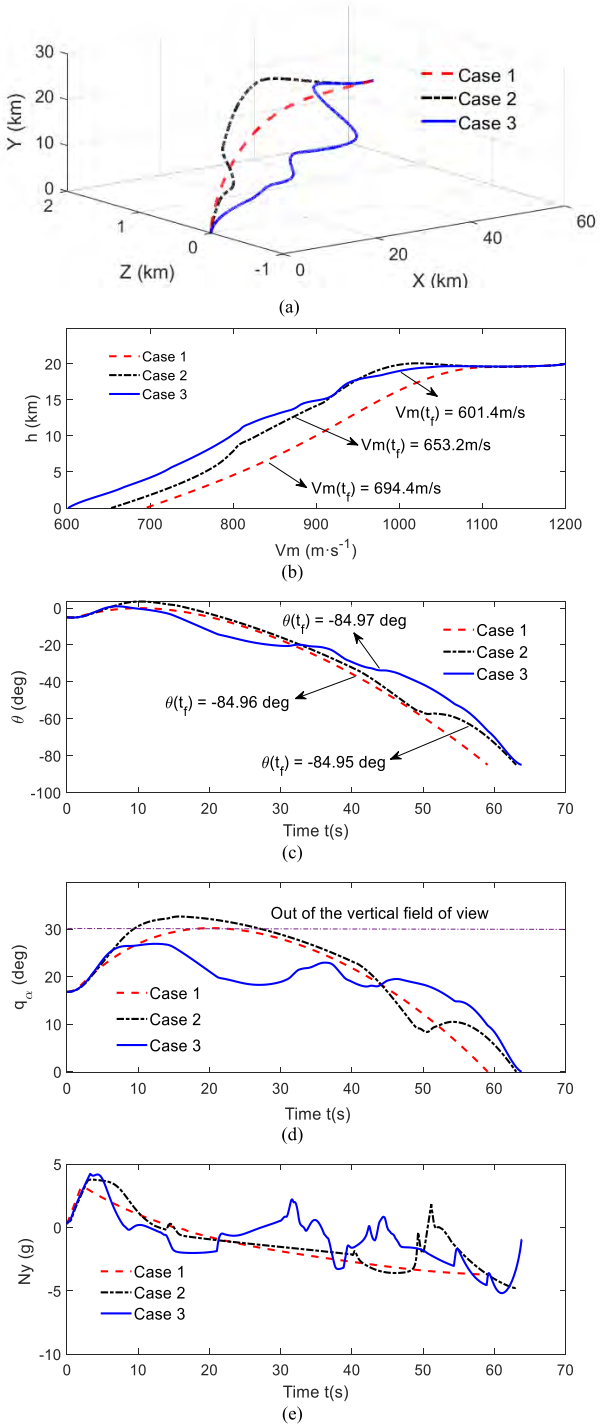

FIGURE 11. Comparison results of different guidance schemes in the terminal attack phase. (a) Trajectory. (b) Altitude vs. velocity. (c) Flight-path angle vs. time. (d) Deviation of the vertical field of view vs. time. (e) Acceleration vs. time.

Figure 12 shows the simulation results of the proposed terminal guidance scheme when the target moves at a speed of 20 m/s and its heading angles are taken as 0 deg (case 1), 90 deg (case 2), 180 deg (case 3) and 270 deg (case 4), respectively. The statistical results of the simulation are given in Table 3, in which 'a' represents the case with no

TABLE 2. Simulation conditions for the terminal attack phase.

Name	Value	Name	Value
Range (km)	50	Flight path angle (deg)	-5
Altitude (km)	20	Velocity (m/s)	1200

TABLE 3. Statistical results for moving targets.

		Impact angle (deg)	Impact velocity (m/s)	Miss distance (m)
1	a	-87.5189	599.7043	0.5767
	b	-84.9765	599.3009	0.8952
	c	-93.4971	599.7416	11.9475
2	a	-84.5685	597.2065	0.8578
	b	-84.5276	597.4301	0.7845
	c	-86.7380	597.6130	0.4259
3	a	-82.4589	599.6977	0.7517
	b	-84.9858	596.8625	0.4979
	c	-84.9775	596.7113	0.5337
4	a	-84.2519	596.5625	0.7076
	b	-84.5215	599.5145	0.8530
	c	-86.4915	597.0289	0.4473

compensation for the target motion information (that is to say, we do not know the target information and think $\gamma_R = \gamma_M$ and $\kappa = 1$.), 'b' represents the case which has compensation for target motion information and uses Eq. (49) to calculate the velocity ratio, and 'c' represents the case which has compensation for target motion information and uses $\beta = V_T/V_M$ to calculate the velocity ratio. It can be seen from Fig. 12b that all the above schemes have little effect on the accuracy of impact velocity, but have obvious influence on the accuracy of impact angle. It should be noted that the relative velocity vector must lie on the line of sight for a successful capture. Therefore, when the vehicle hits the moving target without target motion information compensation, the accuracy of impact angle control will be reduced. If $\beta = V_T/V_M$ is used to calculate the velocity ratio, it will reduce the calculation accuracy of the relative flight-path angle. Then it will reduce the accuracy of impact angle. The results in Fig. 12c and Table 3 validate the conclusion. Through the above analysis, it is known that the accuracy of impact angle control can be greatly improved by using the target motion information to compensate the proposed guidance scheme. The curves of the weight coefficient are shown in Fig. 12d. In the first half of the trajectory, the weight coefficients are taken as small values to force down the trajectories rapidly and stable the field of view tracking. In the second half of the trajectory, the values of the weight coefficient are gradually increased to complete the angle control as soon as possible. It is consistent with the design results.

B. GUIDANCE PERFORMANCE FOR ALL THE REENTRY TRAJECTORIES

Figure 13 gives the simulation results of the reentry phase for various terminal velocity at the handover point. In addition, in order to ensure successful terminal attack phase flight,

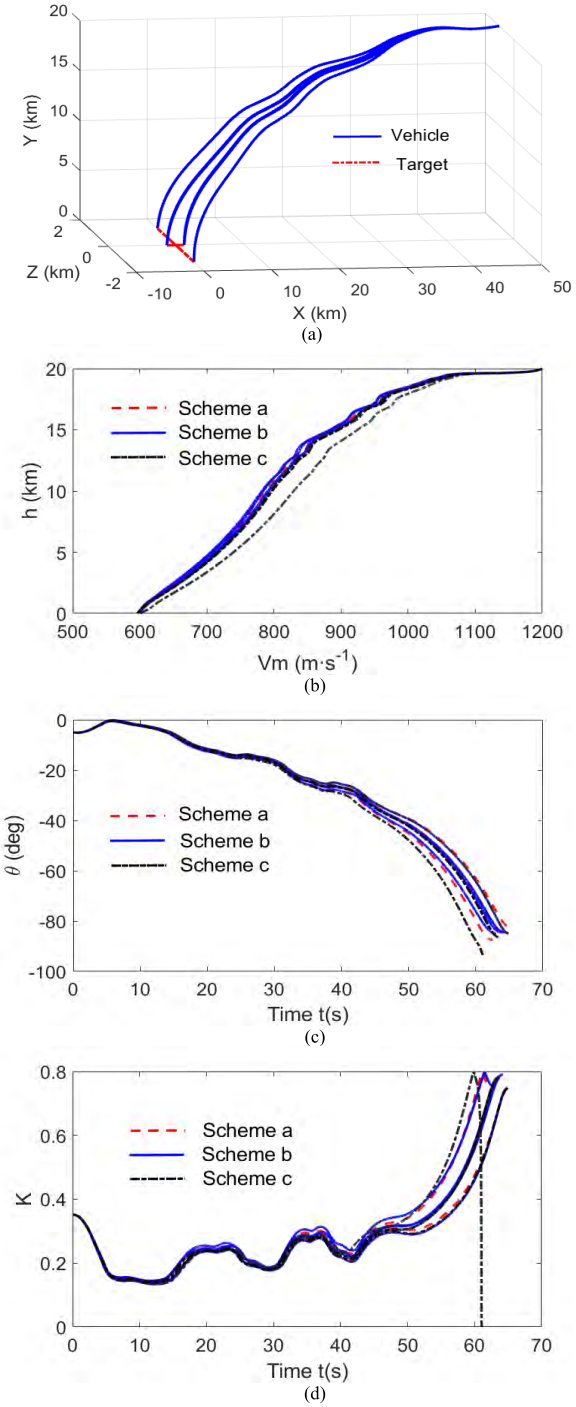

FIGURE 12. Verification of the proposed terminal guidance performance against moving targets. (a) Trajectory. (b) Altitude vs. velocity. (c) Flight-path angle vs. time. (d) Weight coefficient vs. time.

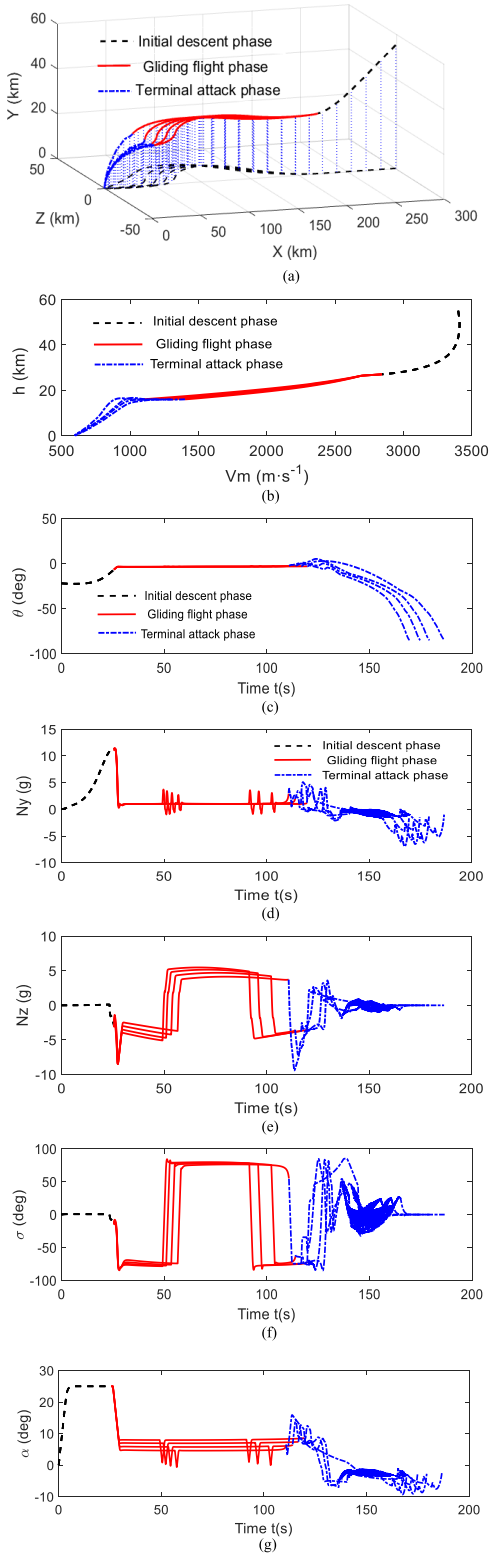

FIGURE 13. Reentry guidance performance for different terminal velocity constraints at the handover point. (a) Trajectory. (b) Altitude vs. velocity. (c) Flight-path angle vs. time. (d) Longitudinal acceleration vs. time. (e) Lateral acceleration vs. time. (f) Bank angle vs. time. (g) Angle of attack vs. time.

the altitude and range-to-go at the handover point are taken as 16 km and 50 km, respectively. The initial reentry conditions and simulation statistics are given in tables 4 and 5 respectively. Due to the short reentry range, it can be seen

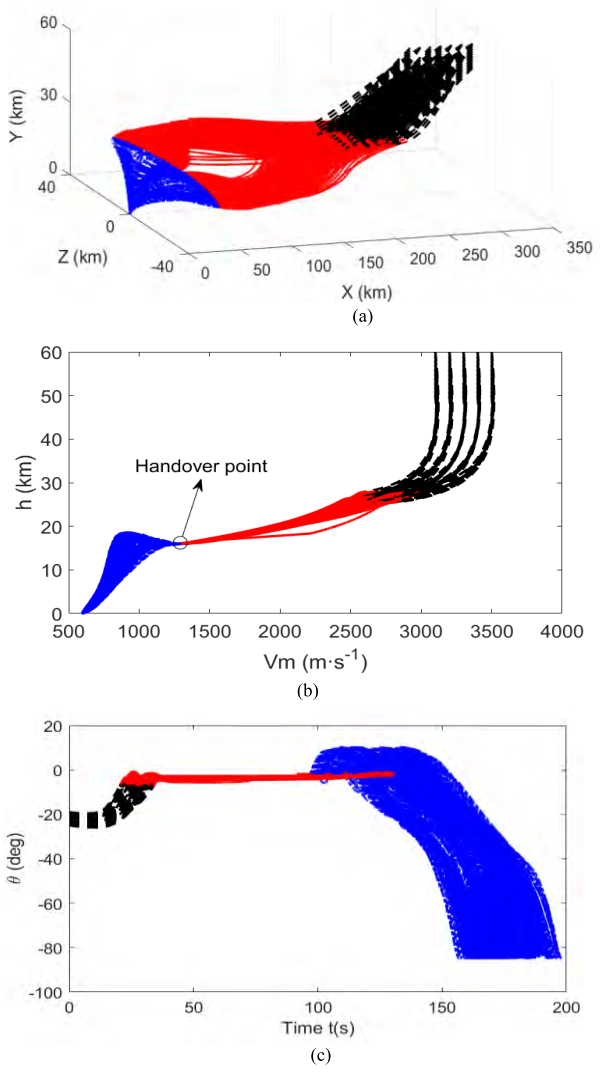

FIGURE 14. Statistical results of 300 fire tests. (a) Trajectory. (b) Altitude vs. velocity. (c) Flight-path angle vs. time.

TABLE 4. Initial conditions for the reentry phase.

Name	Value	Name	Value
Range (km)	300	Flight-path angle (deg)	-22
Altitude (km)	55	Velocity (m/s)	3400

from Fig. 13a that all the trajectories of the vehicle are similar to the C-shaped curves. Combining the velocity-altitude curves in Fig. 13b and the results in Table 5, it can be seen that under different terminal velocity constraints at the handover point, the terminal velocity errors at the handover point, the impact velocity errors, the impact angle errors and miss distance are less than 5 m/s, 5 m/s, 0.04 deg and 1.2 m, respectively. It can be seen from Figs. 13d, 13e, 13f and 13g that all the curves of the acceleration, bank angle and angle of attack meet the corresponding process constraints.

In order to verify the robustness of the proposed guidance algorithm, based on the deviation ranges of the given

TABLE 5. Statistical results for different terminal velocity constraints at the handover point.

Variable	V_{MF} (m/s)	h_{MF} (km)	s_{MF} (km)	V_F (m/s)	θ_F (deg)	r_f (m)
Desired value		16	50	600	-85	<6
1100	1096	16.02	50.2	602.8	-84.95	0.99
1200	1203	16.02	50.3	603.6	-84.96	0.90
1300	1296	16.01	50.1	602.8	-84.95	0.89
1400	1403	16.01	49.8	596.3	-84.97	0.97
1500	1497	16.02	50.2	597.6	-84.68	1.17

TABLE 6. The deviation range of different variables.

Name	Value	Unit
Atmospheric density	$\pm$ 10%	kg/m^3
Lift coefficient	$\pm$ 15%	
Drag coefficient	$\pm$ 15%	
Initial altitude	55 ± 3	km
Initial velocity	3300 ± 200	km
Initial range	300 ± 30	km
Initial flight-path angle	-22 ± 3	deg
Initial heading angle	180 ± 10	deg

variables in Table 6, we randomly select 300 groups of deviation combinations for simulation verification. The flight trajectories, velocity-altitude curves and flight-path angle curves are shown in Fig. 14. Except for four failures, the vehicle hit the target as required for all other cases. The simulation results show that the proposed guidance scheme has loose initial conditions and good robustness.

VI. CONCLUSIONS

A short-range reentry guidance algorithm based on the C-shaped trajectory is proposed to achieve precise reentry strike. The trajectory is divided into reentry gliding phase and terminal attack phase, which are designed separately. In the reentry gliding phase, by using the hybrid guidance scheme, the trajectory convergence characteristic is good, the search speed is fast, and the constraints at the handover point are realized with high precision. In the terminal attack phase, by combining the derived generalized biased PN guidance algorithm and the numerical predictor corrector method, the relationship among PN command, angle control command and velocity control command is well coordinated to ensure that the vehicle can complete forcing down the trajectory under the vertical field of view constraint, while achieving high impact velocity and impact angle control accuracy. Although the impact angle control guidance law requires a small amount of target motion information, the compensation information slightly affects the accuracy of the angle control. The simulation results also verified that the proposed guidance scheme is insensitive to the initial conditions and exhibits a good robustness. However, the influence of the coupling between the longitudinal and lateral channels on the guidance performance is not taken into account when

deriving the reentry guidance scheme. In-depth analysis of this characteristic needs to be carried out in the future, to further improve the guidance performance of the proposed guidance scheme.

REFERENCES

[1] J. C. Harpold and C. A. Graves, "Shuttle entry guidance," *J. Astronaut. Sci.*, vol. 27, no. 3, pp. 239–268, Jul. 1979.
[2] J. C. Harpold and D. E. Gavert, "Space shuttle entry guidance performance results," *J. Guid., Control, Dyn.*, vol. 6, no. 6, pp. 442–447, Nov. 1983.
[3] A. J. Roenneke and A. Markl, "Re-entry control to a drag-vs-energy profile," *J. Guid., Control, Dyn.*, vol. 17, no. 5, pp. 916–920, Sep. 1994.
[4] H. F. Li and L. Xie, "Reentry guidance law design for RLV based on predictor method," *J. Beijing Univ. Aeronaut. Astronaut.*, vol. 35, no. 11, pp. 1344–1348, Nov. 2009.
[5] E. M. Yong, W. Q. Qian, and K. F. He, "An adaptive predictor–corrector reentry guidance based on self-definition way-points," *Aerosp. Sci. Technol.*, vol. 39, pp. 211–221, Dec. 2014.
[6] P. Lu, "Entry Guidance: A unified method," *J. Guid., Control, Dyn.*, vol. 37, no. 3, pp. 713–728, Feb. 2014.
[7] J. P. Masciarelli *et al.*, "An analytic aerocapture guidance algorithm for the mars sample return orbiter," in *Proc. Atmos. Flight Mech. Conf.*, Denver, CO, USA, Aug. 2000, p. 4116.
[8] J. F. Hamel and J. D. Lafontaine, "Improvement to the analytical predictor-corrector guidance algorithm applied to mars aerocapture," *J. Guid., Control, Dyn.*, vol. 29, no. 4, pp. 1019–1022, Jul. 2006.
[9] A. Joshi, K. Sivan, and S. S. Amma, "Predictor-corrector reentry guidance algorithm with path constraints for atmospheric entry vehicles," *J. Guid., Control, Dyn.*, vol. 30, no. 5, pp. 1307–1318, Sep. 2007.
[10] P. Lu, "Predictor-corrector entry guidance for low-lifting vehicles," *J. Guid., Control, Dyn.*, vol. 31, no. 4, pp. 1067–1075, Jul. 2008.
[11] S. B. Xue and P. Lu, "Constrained predictor-corrector entry guidance," *J. Guid., Control, Dyn.*, vol. 33, no. 4, pp. 1273–1281, Jul. 2010.
[12] Z. J. Shen and P. Lu, "Onboard generation of three-dimensional constrained entry trajectories," *J. Guid., Control, Dyn.*, vol. 26, no. 1, pp. 111–121, Jan. 2003.
[13] C. A. Kluever and C. A. Neal, "Approach and landing range guidance for an unpowered reusable launch vehicle," *J. Guid., Control, Dyn.*, vol. 38, no. 11, pp. 2057–2066, Mar. 2015.
[14] W. Yu and W. C. Chen, "Trajectory-shaping guidance with final speed and load factor constraints," *ISA Trans.*, vol. 56, pp. 42–52, May 2015.
[15] H. Zhou, T. Rahman, and W. C. Chen, "Impact angle and impact velocity constrained terminal guidance for stationary target," *Aircr. Eng. Aerosp. Technol., Int. J.*, vol. 87, no. 5, pp. 454–464, Sep. 2015.
[16] Z. Hanyuan and C. Kejun, "Velocity control of maneuvering reentry vehicle," *J. Nat. Univ. Defense Technol.*, vol. 15, no. 2, pp. 11–17, 1993.
[17] P. Y. Liu *et al.*, "A coning motion-based guidance law for guided rocket with velocity control," *Acta Aeronaut. Astronaut. Sin.*, vol. 35, no. 4, pp. 933–941, 2014.
[18] J. H. Song, "A velocity control method of the reentry vehicle based on flight simulation," *Missiles Space Veh.*, vol. 318, no. 2, pp. 4–7, 2012.
[19] Q. Li *et al.*, "Maneuvering-deceleration guidance algorithm based on atmosphere estimation for reentry vehicle," *Acta Armamentarii*, vol. 34, no. 9, pp. 1091–1096, 2013.
[20] L. Wang, J. Yu, Y. Mei, and Y. Wang, "Guidance law with deceleration control for moving-mass reentry warhead," *Proc. Inst. Mech. Eng., G, J. Aerosp. Eng.*, vol. 230, no. 14, pp. 2639–2653, Dec. 2016.
[21] P. Lu, D. B. Doman, and J. D. Schierman, "Adaptive terminal guidance for hypervelocity impact in specified direction," *J. Guid., Control, Dyn.*, vol. 29, no. 2, pp. 269–278, Mar. 2006.
[22] A. Ratnoo and D. Ghose, "Impact angle constrained interception of stationary targets," *J. Guid., Control, Dyn.*, vol. 31, no. 6, pp. 1816–1821, Nov. 2008.
[23] K. S. Erer and O. Merttopçuoglu, "Indirect impact angle control against stationary targets using biased pure proportional navigation," *J. Guid., Control, Dyn.*, vol. 35, no. 2, pp. 700–703, Mar. 2012.
[24] C. H. Lee, T. H. Kim, and M. J. Tahk, "Interception angle control guidance using proportional navigation with error feedback," *J. Guid., Control, Dyn.*, vol. 36, no. 5, pp. 1556–1561, Mar. 2013.
[25] H. Y. Zhao, *Spacecraft Reentry Dynamics Guidance*, Changsha, China: Press Natl. Univ. Def. Technol, 1997.
[26] Z. Jiang, L. Sun, J. Wang, and Z. Huang, "Environmental parameter Online identification and its application in gliding guidance," *J. Natl. Univ. Def. Technol.*, vol. 40, no. 2, pp. 48–54, Apr. 2018.
[27] C. Lai, W. Wang, Z. Liu, T. Liang, and S. Yan, "Three-dimensional impact angle constrained partial integrated guidance and control with finite-time convergence," *IEEE Access*, vol. 6, pp. 53833–53853, 2018.
[28] Z. Qin, X. Qi, and Y. Fu, "Terminal guidance based on Bézier curve for climb-and-dive maneuvering trajectory with impact angle constraint," *IEEE Access*, vol. 7, pp. 2969–2977, 2018.
[29] L. Ran, W. Qiuqiu, T. Wangchun, and Z. Yijie, "Adaptive weighting impact angle optimal guidance law considering seeker's FOV angle constraints," *J. Syst. Eng. Electron.*, vol. 29, no. 1, pp. 142–151, Feb. 2018.
[30] H.-G. Kim, J.-Y. Lee, and H.-J. Kim, "Look angle constrained impact angle control guidance law for homing missiles with bearings-only measurements," *IEEE Trans. Aerosp. Electron. Syst*, vol. 54, no. 6, pp. 3096–3107, Dec. 2018.
[31] M.-G. Seo, C.-H. Lee, and M.-J. Tahk, "New design methodology for impact angle control guidance for various missile and target motions," *IEEE Trans. Control Syst. Technol*, vol. 26, no. 6, pp. 2190–2197, Nov. 2018.
[32] K. S. Erer and M. K. Ozgoren, "Control of impact angle using biased proportional navigation," in *Proc. AIAA Guid., Navig., Control Conf.*, Boston, MA, USA, 2013, p. 5113.

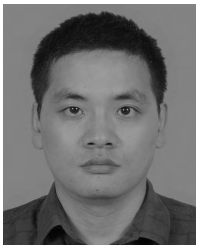

RONGGANG WANG was born in Xi'an, China. He received the B.S. and M.S. degrees in aerospace designing form Northwestern Polytechnical University (NPU), Xi'an, in 2011 and 2014, respectively, where he is currently pursuing the Ph.D. degree in aerospace designing. His research interests include terminal guidance law, reentry guidance, deceleration control, automatic control, cooperative guidance, midcourse guidance, and interception guidance.

SHUO TANG received the B.S., M.S., and Ph.D. degrees in aerospace engineering from Northwestern Polytechnical University, Xi'an, China, in 1982, 1985, and 1988, respectively, where he is currently a Professor. His research interests include aerospace vehicle design, flight dynamics and control, flight simulation and virtual prototyping technology, guidance and control technology of spacecraft, and hypersonic dynamics and integrated design.

DONG ZHANG received the B.S. degree from the School of Mathematics and Computer Science, Ningxia University, Yinchuan, China, in 2008, and the M.S. degree from the School of Science and the Ph.D. degree from the School of Astronautics, Northwestern Polytechnical University, Xi'an, China, in 2010 and 2013, respectively, where he is currently an Associate Professor. His research interests include cooperative combat, cooperative control and guidance, and swarm task planning.